



Original Research Article

Green nano bio-synthesis of ZnO/ styrene-butadiene rubber / natural rubber (SBR/ NR) nanocomposite and their assessment by use of curing time and mechanical properties

Monireh Alvand Ghiasvand¹, Sajjad Sedaghat^{2*}, Mohammad Reza Allah Gholi Ghasri¹,
Fereshteh Motiei³, Farrokh Roya Nikmaram¹

¹ Department of Chemistry, Yadegar-e-Imam Khomeini (RAH) Shahre-Rey Branch, Islamic Azad University, Tehran, Iran.

^{2*} Department of Chemistry, College of Science, Shahr-e-Qods Branch, Islamic Azad University, Tehran, Iran

³ Department of Chemistry, College of Basic Science, Tehran North Branch, Islamic Azad University, Tehran, Iran

Received: 2024-11-01

Accepted: 2025-01-23

Published: 2025-01-24

ABSTRACT

Zinc oxide nanoparticles (ZnO NPs) were synthesized using *Aloysia Citrodora* leaf water extract as a reducing and capping agent in an alkaline medium. UV-visible (UV-Vis) spectroscopy, Fourier transforms infrared (FTIR) spectroscopy, Brunauer–Emmett–Teller (BET), and X-ray diffraction (XRD) were used for the evaluation of the synthesized ZnO NPs, scanning electron microscope (SEM) was further used for analyzing the morphology, size, and thermal stability of the particles. The curing time and mechanical features of styrene-butadiene rubber/natural rubber (SBR/NR) regularities, including ZnO NPs, were studied and matched with SBR/NR by using micro-sized (standard) ZnO. The SBR/NR vulcanizate with 0.5 phr (parts per hundred rubber) ZnO NPs showed enhanced curing and mechanical characteristics related to the SBR/NR vulcanizate with 5 phr standard ZnO. FESEM images showed the uniform distribution and good dispersion of ZnO NPs in the nanocomposite. As a result, the mechanical features of the build-up ZnO NPs packed SBR/NR were enhanced. Therefore, ZnO NPs functioned as a curing activator to increase the resulting characteristics of the SBR/NR vulcanizates. The noteworthy point is that the amount of ZnO NPs consumed has a significant decrease compared to the amount of commercial zinc oxide, which is one of the environmental concerns.

Keywords: SBR - Zinc oxide nanoparticles (NPs) - Curing activator– Vulcanizate

*Corresponding author email address: sajjadsedaghat@yahoo.com

Introduction

Nanotechnology is progressing at an astonishingly fast rate [1]. Nanoparticles are minute particles that range in size from 1 to 100 nanometers. Due to their small size, nanomaterials exhibit unique chemical properties, making them highly versatile for various applications. Two primary methods are employed in producing nanomaterials: top-down and bottom-up approaches [2,4]. The top-down approach involves breaking down bulk materials into nanoscale components through various processes, while the bottom-up approach involves assembling nanomaterials by combining individual particles [5]. These two methods differ significantly in their chemical processes, with the top-down approach often being more costly and involving hazardous chemicals, which can contribute to environmental harm [6]. Accordingly, it is necessary to develop a process that can replace the quandaries modeled by the chemical procedure, and this is where green synthesis comes into play. Green synthesis Investigations concerning the generation of nanomaterials have been concentrated on green synthesis owing to its gross value and eco-friendliness. Green synthesis (also referred to as biological synthesis) can be described as using biomaterials such as plants and their extract to accommodate nanomaterials [7-8]. Green synthesized nanomaterials are economical and environmentally friendly and have physicochemical attributes comparable to those of chemically integrated [9]. Depending on the conditions and objectives, various physical, chemical, and biological processes [10-11] can synthesize zinc oxide. Spark generation depends on surface chemistry, size distribution, particle morphology, and particle reaction in solution. Morphologically, oxide nanoparticles have two crystal structures, hexagonal and cubic. They are more widely used in the industry because of their more stable hexagonal structure compared with the cubic structure at ambient temperature [12]. Among different methods, green synthesis is necessary for forming nanoparticles essentially because it is easy to apply and economical and requires lower production temperature [13]. This approach is also environmentally friendly and biocompatible [14]. Formerly, zinc oxide nanoparticles were successfully synthesized using *Atalantia monophyla*, *Saffron*, *Moringa oleifera*, *Bauhinia tomentosa*, *Seaweed*, *Olea europaea*, *Citrus aurantifolia*, *Anisochilus carnosus*, and *Phlomis* [15-23]. leaf water extract has been further reported. Very little quantity of ordinary ZnO reacts with the accelerator because it has a small particular surface area, and significant volume remains in the rubber vulcanizates. Nevertheless, in a nano-sized ZnO, because of its sizeable particular surface space, an insufficient amount of

ZnO nearly entirely reacts with the accelerator. So minimal quantity of residues can be closely attached to the rubber materials.

The literature includes many studies focused on how ZnO NPs impact different rubber kinds [24-28]. In other research, the use of green synthesized ZnO NPs as a curing activator for vulcanizing SBR and reducing ZnO amount in rubber formulation is discussed [29]. The performance of a rubber compound is hugely determined by how it is vulcanized. Crosslinking or vulcanizing is a method where a significantly solvent plastic compound is transformed into an insoluble elastic case having enhanced mechanical features and properly resisting temperature changes and solvent performance [30]. The ZnO improves vulcanizing or crosslinking when applied as a rubber vulcanization activator [31]. Stearic acid is considered to be able to enhance ZnO activity, thereby speeding up the accelerator and sulfur progress during vulcanization. ZnO is used at 105 tons per year for industrial applications, and about 55 % of ZnO has been employed for rubber applications [32]. One of the most essential advantages of ZnO nanocomposite is their more excellent contact surface than commercial zinc oxide [33]. So in this project, the possibility of synthesizing ZnO NPs from *Aloysia Citrodora* leaf extract as reducing and capping agents is suggested and carried out successfully. Due to its low price and abundance in Iran, *Aloysia Citrodora* leaf was used to synthesize zinc oxide nanoparticles. Thus, the improvement of the technology associated with styrene-butadiene rubber / natural rubber (SBR/ NR) nanocomposite based on green route as a novel process is also made. The nanocomposite produced through this method is cost-effective, lightweight, and biocompatible.

Materials and Methods

Preparation of the leaf extract

Aloysia citrodora leaves were gathered from different parts of Alborz province in Iran. The leaves were cleaned several times with water to eliminate the dust bits and dried light. The dried leaves were then cut and ground for powder.

To prepare the *Aloysia citrodora* leaf extract, 10 g of washed, dried, finely powdered and 100 ml of double-distilled water was mixed. Afterward, the solution was heated for 30 minutes at a temperature of 60 °C using a magnetic stirrer, as a result of which the color of the solution turned

into light yellow (as shown in Fig.1.b). The resulting water extract was moderated to room temperature and cleaned using filter paper (Whatman No.14), which was then collected in the refrigerator for further tests.

Preparing zinc oxide nanoparticles

0.89 grams of zinc acetate dihydrate were dissolved in 100 ml of double distilled water to prepare 2 mM of this solution. Then 20 mL of previously prepared water extract was added to the Zinc acetate dihydrate solution drop by drop at room temperature while stirring up to the color changing from pale green to pale yellow. Then NaOH solution (1M) was added to the reaction vessel until the pH reached 12 (Fig.1. d). The solution was centrifuged for 20 min at 4000 rpm, and the precipitate was collected. The precipitates were washed with distilled water and ethanol twice and were then dried in an air oven overnight at 80°C. The prepared solids were heated in a furnace at 500°C for three hours. Biomolecules existing in the *Aloysia Citrodora* water extract acted as capping agents, leading to the formation of the ZnO NPs in the alkaline medium.



Figure 1 a) *Aloysia Citrodora* plant b) *Aloysia Citrodora* water extract c) Zinc acetate Solution d) biosynthesized ZnO NPs using *Aloysia Citrodora* water extract

Rubber Materials

All the rubber materials employed in this study are as follows: natural rubber (NR.; SMR-20, Lee Rubber Company, Singapore), styrene-butadiene rubber (SBR; SBR-1502, Bandar Imam

petrochemical company, Bandar Imam, Iran), Zinc oxide (particular surface area $5 \text{ m}^2/\text{g}$, Rangin 99.9%), carbon black grade N330 (pars carbon black (Iran)), stearic acid (KLK oleo Malaysia), insoluble sulfur S (Iran Tsedak production company), accelerator Tetramethyl Thiuram disulfide TMTD (Liuyang Sanji Chemical Co., Ltd, China), and accelerator N-cyclohexyl-2-benzothiazole sulfonamide CBS (Liuyang Sanji Chemical Co., Ltd, China).

Instrumentation

The scanning electron microscopy (SEM) images were obtained using a JSM 6700F instrument. The X-ray diffraction (XRD) pattern of ZnO nanoparticles (NPs) was analyzed using an Xpert-Pro Analytical X-ray diffractometer. The surface morphology of the nanocomposite was examined using a TESCAN MIRA3 device equipped with Field Emission Scanning Electron Microscopy (FESEM). The surface area of ZnO NPs was determined using a BET Belsorp mini x (Japan) specific surface and pore size analyzer. Cure properties of various rubber stocks were measured using a Monsanto rheometer R-100 at three arcs and a temperature of 140°C . Tensile properties, including modulus at 100% (M100) and 300% (M300) elongation, tensile strength (T.S.), and elongation at break (E.B. in %), were evaluated using dumbbell-shaped test pieces on a tensile tester. The samples were cured under pressure at 140°C for the optimal cure time (t_{90}) and then allowed to rest at room temperature for 24 hours before testing, following ASTM D412 standards. The hardness (Shore A) of the vulcanizates was measured using a hardness tester in accordance with ASTM D2240-97.

Preparation of SBR/NR compounds

According to the formulation in Table 1, all materials were weighed and prepared for mixing. A two-roll mixing mill ground the SBR/NR; after setting the ZnO, the addition of stearic acid was carried out, and the grinding was repeated. Next, the accelerator and sulfur were mixed with the rubber matrix for approximately 20 min. The overall accelerator mass was set to 10 mmol for each 100 g of the rubber. This technique was performed one more time to provide SBR/NR nanocomposites, including various ZnO NPs. Table 1 presents the mixing structure of various parts. For various mixes, SBR/NR indicates styrene-butadiene rubber/ natural rubber. SBR/NR-0.5 NZnO (SN0.5) (in which the number shows the quantity in phr, N represents nanoparticles, I refers to industrial particles ZnO) represents SBR/NR vulcanizate which in turn includes 0.5 phr

ZnO NPs, SBR/NR 1 phr ZnO NPs (SN1), SBR/NR 2 phr ZnO NPs (SN2) and SBR/NR 5 phr industrial ZnO (SN5I). The optimal amount is obtained in the industry of 5 phr of zinc oxide [25].

Table 1. The formulation of studied vulcanizates in parts per hundred parts of rubber (phr)

Formulation	Compound selection			
	SN0.5	SN1	SN2	SN5I
SBR (1502) /NR (SMR-20)	100	100	100	100
Industrial ZnO	-	-	-	5
Nano ZnO	0.5	1	2	-
Stearic acid	2	2	2	2
TMTD	0.5	0.5	0.5	0.5
Sulfur	1.8	1.8	1.8	1.8
CBS	2	2	2	2
Carbon black (N330 HAF)	10	10	10	10

NR: natural rubber; SBR: styrene-butadiene rubber, NR/SBR blend; All weights are in 100 parts of rubber (phr).

Results and Discussion

Characterization of ZnO nanoparticles

Figure 2 displays the XRD pattern of ZnO nanoparticles (NPs) synthesized through the green route, which aligns with the findings reported in reference [15]. The average crystallite size was calculated using the Debye-Scherrer equation:

$$D = K\lambda / B \cos \theta \text{ (Eq. A.1),}$$

Where D represents the crystallite size, K is a constant close to 1, λ is the X-ray wavelength (0.154 nm), B is the integral half-width, and θ is the Bragg angle. The average crystallite size of the ZnO NPs was determined to be 62 nm. The Scherrer equation is commonly used to estimate crystallite sizes in nanoparticles. Additionally, the surface area of the ZnO NPs was calculated using the equation [33, 34]: $S = \rho L / 6$ where S is the specific surface area, ρ is the density, and L is the average particle size. The surface area of the ZnO NPs was found to be 43.3 m²/g. All peaks observed in Fig. 1 were accurately matched to the hexagonal phase of ZnO, and the narrow, sharp peaks indicated high crystallinity of the nanopowder. The high intensity of the (101) peak suggested anisotropic growth, reflecting a preferred orientation of the crystallites. Analysis of the XRD patterns provided data on peak intensity, position, width, and full width at half-maximum (FWHM). Diffraction peaks at 31.79°, 34.42°, 36.27°, 47.55°, 56.64°, 62.92°, 68.07°, and 69.15° were precisely indexed to the hexagonal wurtzite phase of ZnO. Using Scherrer's formula, the average particle size of the sample was approximately 62 nm, based on the FWHM of the most intense peaks corresponding to the (101) planes at 36.27°. The XRD pattern of the ZnO nanoparticles closely matched the standard reference (JCPDS no. 36-1451).

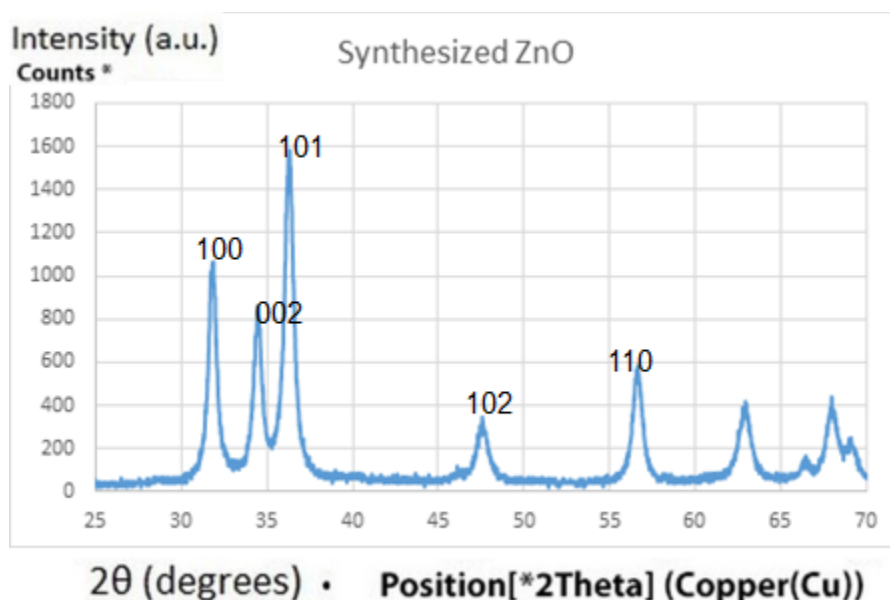


Figure 2. XRD pattern of biosynthesized ZnO nanoparticles

UV-vis spectrometer

Fig. 3 shows the UV-vis spectrometer of the ZnO NPs. At 357 nm, an absorption peak was detected for Zinc oxide nanoparticles, which accords with the findings reported by Paul and Ban [35]. Moreover, Santhoshkumar et al. [36] demonstrated that the UV absorption spectra having wavelengths varying from 300 to 500 nm distinguished the visible attributes related to ZnO NPs.

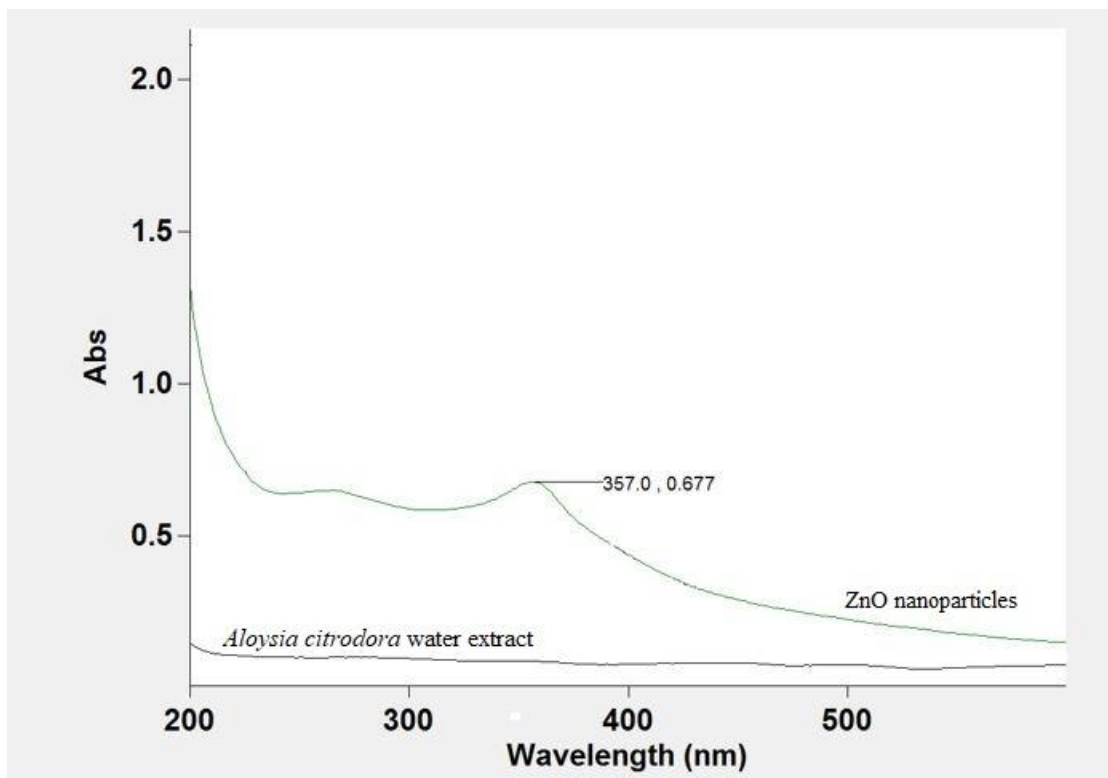


Figure 3. UV-Vis spectra of ZnO nanoparticles and *Aloysia citrodora* water extract

Fourier transform infrared spectroscopy (FTIR)

To study the functional groups and specify how ZnO NPs were created, the Fourier transform infrared spectroscopy was utilized. However, the FTIR spectrum of *Aloysia Citrodora* water leaf extract and the zinc oxide was reported to range from 420 cm^{-1} to 3500 cm^{-1} . Two samples were observed at the (a) powder of *Aloysia citrodora* water extract and (b) ZnO NPs synthesized via *Aloysia Citrodora* water leaf extract. The $3400\text{-}3463\text{ cm}^{-1}$ is related to the stretching and bending vibrations for hydroxyl (O-H) groups related to water molecules present in the samples. The

vibration bands detected at 2926, 2553, 1625, 1405, 1116, and 618 cm^{-1} were all related to the biomolecules presenting in the leaf water extract [37]. As shown in Fig. 3.b, the peaks related to biomolecules are removed, dealing with the attending in the synthesizing process of ZnO NPs.

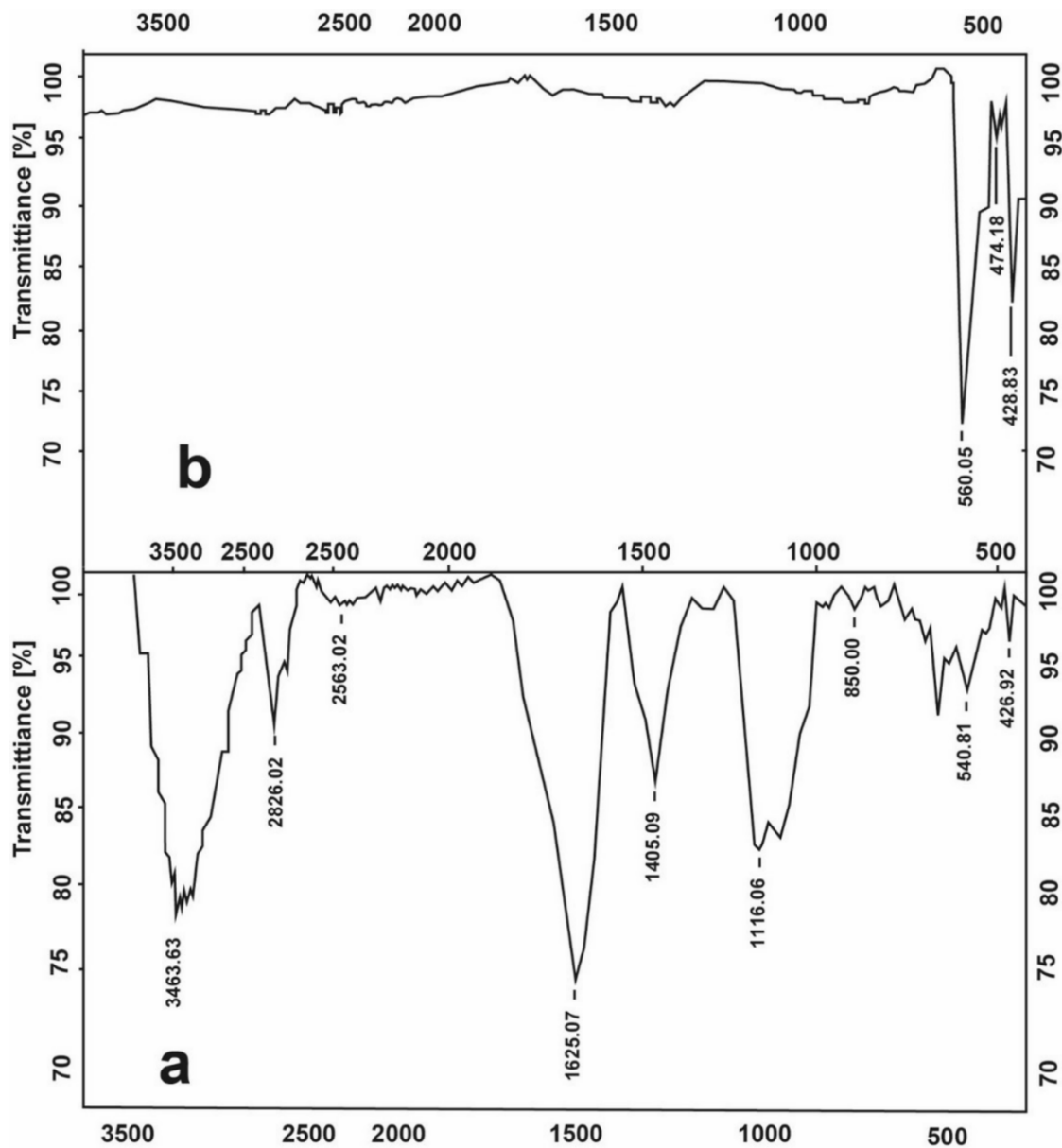
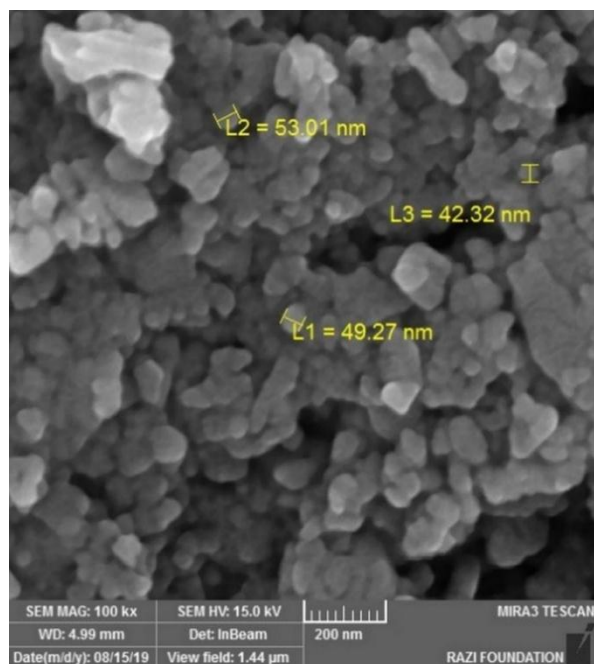


Figure 4. FT-IR spectra of (a) powder of *Aloysia citrodora* water extract,

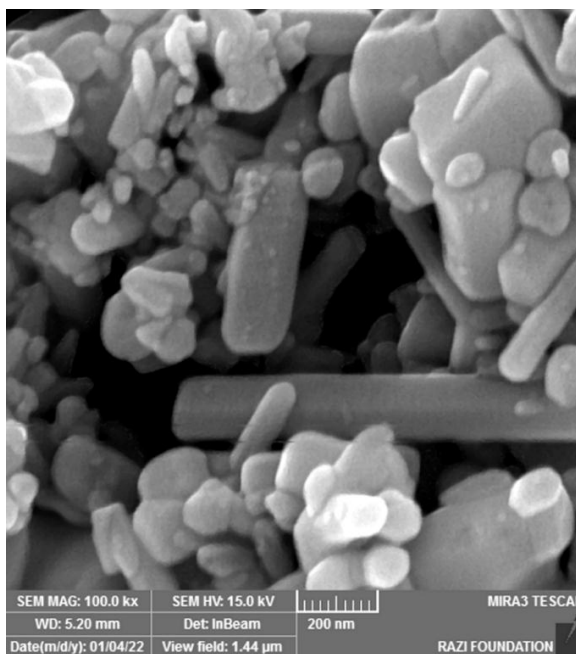
(b) ZnO NPs synthesized by *Aloysia citrodora* water extract

Scanning Electron Microscope (SEM)

Fig.5 shows the comparison between SEM images of (a) ZnO NPs and (b) micro ZnO. Fig.5. (a) show how SEM was performed at various magnifications. The created ZnO NPs were shaped spherical. The size of the ZnO NPs ranged between 40 and 180 nm. The particles were well distributed, indicating aggregation due to their immense surface energy [38]. Nevertheless, the boundaries between individual crystallites were observable. It can be seen that the outcomes are teeny, aggregated nanoparticles with spherical shapes. By looking at the images of micro ZnO Fig.5.(b), can be seen in rod shapes and on larger dimensions. The surface of zinc oxide nanoparticles was observed to be smoother, more homogeneous without agglomeration (due to the green synthesis method of the ZnO NPs), and more spherical [39].



a) SEM image of ZnO NPs



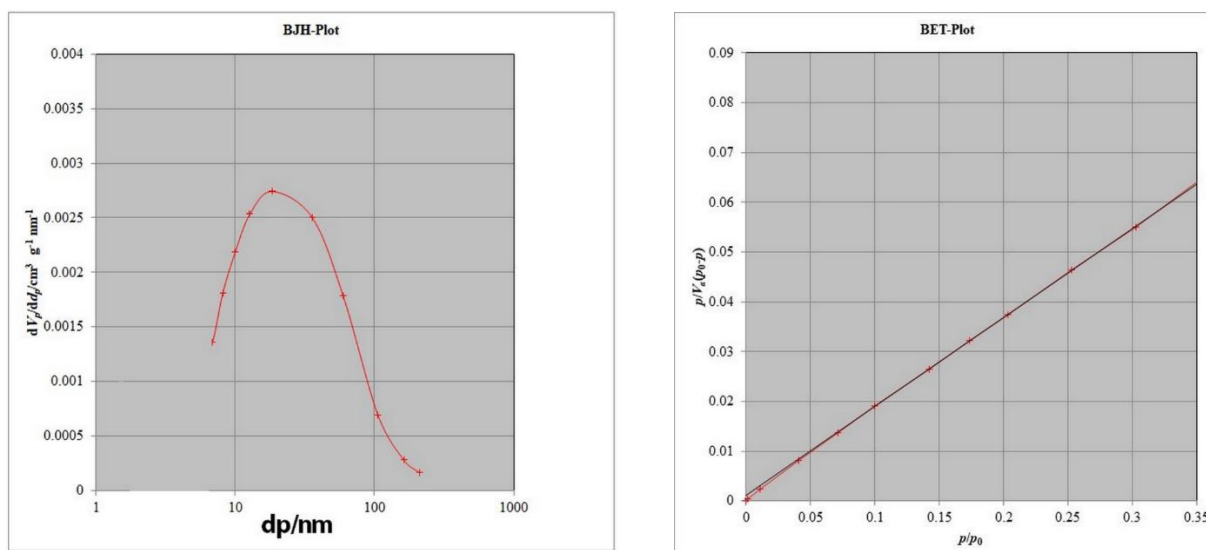
b) SEM image of micro ZnO

Figure 5. SEM images of ZnO NPs and micro ZnO

Brunauer– Emmett–Teller (BET)

The specific surface areas are detected in a Brunner Emmett-Teller (BET) manner. Surface areas of ZnO NPs were contained by a Belsorp mini x (Japan) specific surface and a pore size analyzer. Estimated by BET, the surface areas of ZnO NPs are $24.212 \text{ m}^2/\text{g}$, the average pore diameter is 44.942 nm , and total pore volume ($p/p_0=0.9900$) is $0.027851 \text{ [cm}^3 \text{ g}^{-1}]$ (Figure 6a, b) [40].

The porous and textural properties of ZnO NPs and micro ZnO are shown in Table 2. The green synthesized ZnO NPs resulted in the unique properties of the specific surface area (S_{BET}), pore volume (V_{micro}), average pore diameter (D_{average}), and total volume (V_{total}). Compared with the micro ZnO, the ZnO NPs showed a significant increase in S_{BET} , V_{total} , and V_{micro} .



(a) pore size dispersion of ZnO NPs (b) N_2 adsorption/desorption isotherm of ZnO NPs

Figure 6. BET results of ZnO NPs and micro ZnO

Table 2. Physical properties of ZnO NPs, and micro ZnO adsorbents by BET Analysis

sample	$S_{\text{BET}} (\text{m}^2 \text{ g}^{-1})$	$V_{\text{total}} (\text{cm}^3 \text{ g}^{-1})$	$V_{\text{micro}} (\text{cm}^3 \text{ g}^{-1})$	$D_{\text{average}} (\text{nm})$
ZnO NPs	24.212	0.2117	5.5628	44.942
micro ZnO	4.6476	0.027851	1.0678	23.97

Characterization of the synthesized nanocomposite

Cure qualities of SBR/NR vulcanizates

Utilizing both ZnO and the accelerator influenced the vulcanization speed significantly. Fig. 7 depicts the rheometric curves related to SBR/NR vulcanizates based on the quantity of ZnO in vulcanization. As shown in Table 3, t_{s2} (scorch time), t_{90} (optimum cure time), and cure rate index (CRI) represent the cure properties. Because of its larger surface area, ZnO NPs affected vulcanization more significantly than micro ZnO. Concerning the curing speed, t_{s2} and t_{90} increased with the increase in the ZnO content, while the CRI reduction was caused by the higher amount of time needed to form the chelate complex having more Zn ion. The curing variables related to SBR/NR vulcanizates were calculated at 140°C with both nano and Industrial ZnO present (Table 3). Based on the results, the SBR/NR vulcanizate with 5 phr industrial ZnO had a significantly higher optimum curing time (t_{90}) than the SBR/NR vulcanizate comprising 0.5 phr ZnO NPs. This implies that ZnO NPs, as compared with Industrial ZnO, were a more effective crosslinking element and a more optimal curing activator for vulcanizing SBR/NR. The cure rate index (CRI) related to various SBR/NR vulcanizates also corroborated the effectiveness of the crosslinking associated with ZnO NPs. The CRI amount was more inclusive for SBR/NR vulcanizate comprised of 0.5 phr ZnO NPs (SN0.5) equivalent to SBR/NR vulcanizate with 5 phr Industrial ZnO (SN5I). The ZnO NPs particular surface area was more significant than Industrial ZnO. As a result, when utilized as a cure activator, ZnO NPs reacted efficiently, due to their enhanced interfacial area, with stearic acid. This occurs typically in the disposition of a great mass related to the molecules of zinc stearate. Therefore, the CRI amount increased significantly after including 0.5 phr ZnO NPs and SBR/NR involving the amount of SBR/NR vulcanizate with 5 phr Industrial ZnO [41].

Compared to industrial ZnO, ZnO NPs have a larger particular surface area; thus, the reaction of the latter with stearic acid and accelerator was much faster, generating more zinc accelerator complexes. After that, active sulfurating agents reacting with the rubber chain's allylic sites formed vast crosslink. ΔH indirectly showed the crosslink density of the SBR/NR vulcanizates (Table 3). These results confirm the data observed for hardness. The synthesized ZnO NPs increased the pH of the mixture, thereby increasing the curing speed.

On the other hand, as can be seen, the high surface areas of ZnO NPs increase the formation rate of the accelerator-zinc oxide complex, thus reducing the curing time [42].

The formation of ZnO NPs, stearic acid, accelerators and sulfur complex are the essential, and vital steps in the curing mechanism. ZnO NPs act both as an activator and as a catalyst in the polymer matrix. Due to the increase in the surface contact of zinc oxide nanoparticles, based on the results of BET in Figure 6 and Table 2, the surface areas of ZnO NPs are $24.212 \text{ m}^2/\text{g}$, so it can be concluded that the decrease in the curing time can increase the adsorption of the zinc accelerator complex with the polymer chains. On the other hand, as the surface area of ZnO NPs particles increased, due to the better interaction between the polymer chains and nano ZnO NPs particles, the crosslink became faster and the curing time shorter. The larger surface area and the smaller size of ZnO NPs particles are anticipated to have a better distribution, as shown in FESEM images of ZnO NPs in Figure 9 [43].

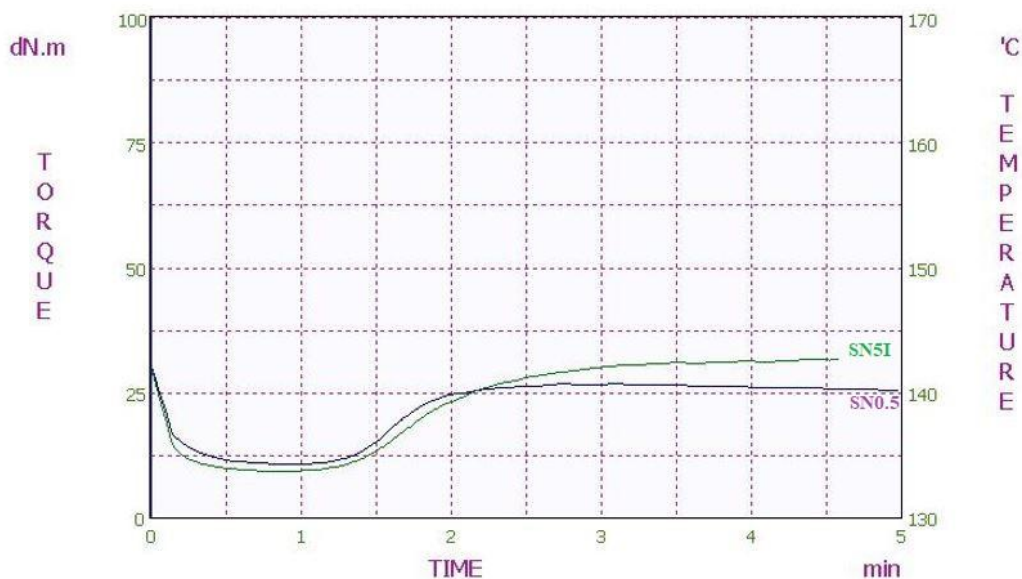


Figure 7. Rheometer curves of SBR/NR vulcanizates as a purpose of ZnO content at 140 °C.

Table 3. Cure characteristics of SBR/NR vulcanizates in the presence of ZnO NPs and Industrial ZnO

Compound selection	Optimum cure time, t_{90} (min)	Scorch time, ts_2 (min)	Cure rate index, CRI = $100/(t_{90} - t_{S2})$ (min^{-1})	$\Delta H = M_H - M_L$
SN0.5	2.07 ± 0.50	1.20 ± 0.25	95.85	22.39
SN5I	2.49 ± 0.50	1.21 ± 0.25	62.68	16.15

Mechanical properties of SBR/NR vulcanizates

Tensile and Elongation test

By ASTM D412, dumbbell-shaped specimens were prepared and tested using a Monsanto T10 tensometer. The average of three measurements was taken, with specimens having a thickness of 2.0 ± 0.2 mm. Testing was conducted at room temperature (23 ± 2 °C) and a relative humidity of $50 \pm 5\%$. Before testing, the specimens were conditioned for a minimum of 24 hours. The hardness of each composite was measured using a Shore A durometer tester following ASTM D 2240-97 standards [44, 45]. The effectiveness of ZnO during vulcanization can be enhanced by increasing the contact area between ZnO particles and organic accelerators. This contact depends on several factors, including the size, shape, and specific surface area of the ZnO particles used. Among these, specific surface area, which is influenced by particle size, plays a crucial role in determining the activity of ZnO particles. Industrial-grade ZnO particles typically have a specific surface area of $4.6476 \text{ m}^2/\text{g}$, while ZnO nanoparticles exhibit a significantly larger specific surface area of $24.212 \text{ m}^2/\text{g}$, making them more effective in comparison[46]. Figure 8 illustrates the differences in mechanical properties between the SN0.5 and SN5I samples. An increase in the modulus value was observed in the SBR/NR nanocomposite compared to the SBR/NR vulcanizate containing industrial ZnO. It is hypothesized that the green-synthesized nano ZnO, due to its large specific surface area and uniform distribution within the rubber matrix, acts as a reinforcing filler during the vulcanization of SBR/NR. Table 4 lists the tensile strength (TS), stress at 100% elongation (M100), stress at 300% elongation (M300), elongation at break (EB), and hardness (Shore A). The superior performance of ZnO nanoparticles in SBR/NR vulcanization compared to ZnO microparticles highlights the enhanced activity of nanoparticles. The properties of SBR/NR vulcanizates containing 0.5 phr of ZnO nanoparticles were notably improved, attributed to the

higher specific surface area of the nanoparticles, which promotes better dispersion and stronger interactions with the rubber components. The tensile strength analysis of the nanocomposite with 0.5 phr of ZnO nanoparticles revealed an increase in elongation at break compared to the sample with industrial ZnO microparticles. Additionally, the hardness of the sample containing ZnO nanoparticles increased, likely due to the improved dispersibility of the nanoparticles, which enhances interactions within the rubber matrix. Overall, the mechanical and curing properties of the rubber were enhanced with the inclusion of ZnO nanoparticles. This improvement is likely due to the larger surface area of the nanoparticles, which provides more active sites for interactions between the organic accelerator and rubber components.

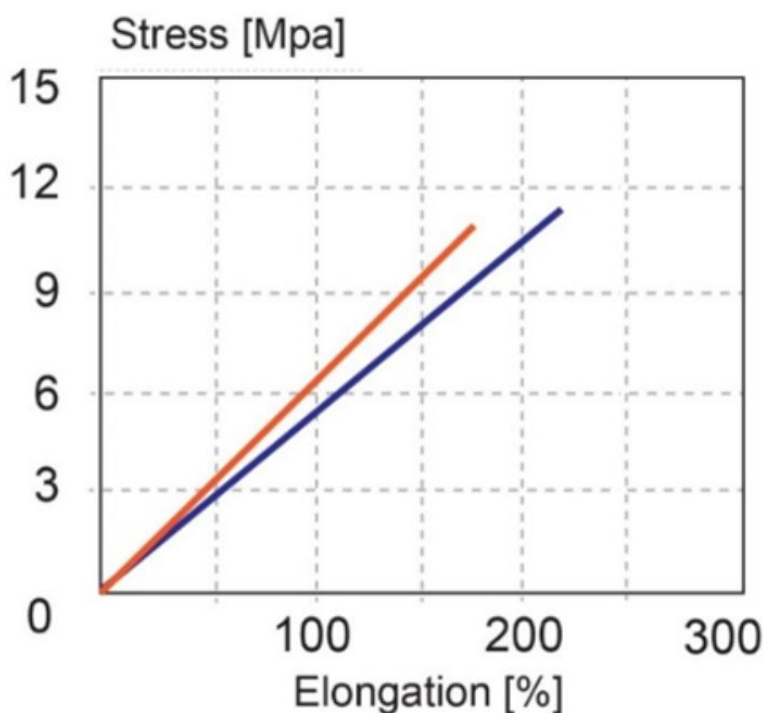


Figure 8. Tensile strength (TS), elongation at break (EB) of SBR/NR vulcanizates activated with ZnO NPs and industrial ZnO

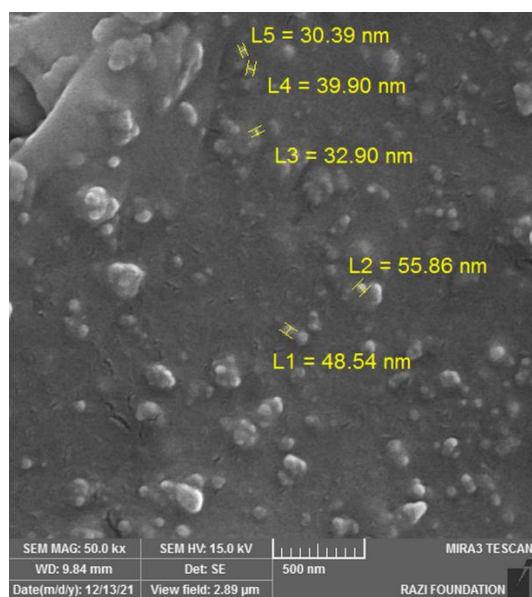
Field emission scanning electron microscopy (FESEM)

Field emission scanning electron microscopy FESEM was accomplished to study the surface morphology and form of the synthesized nanocomposites. Figure 9. (a) shows FESEM of the cross-sectional area of NR/SBR alloy dispersed samples containing ZnO nanoparticles broken down in liquid nitrogen. Zinc oxide particles appear as small white dots in the images. These

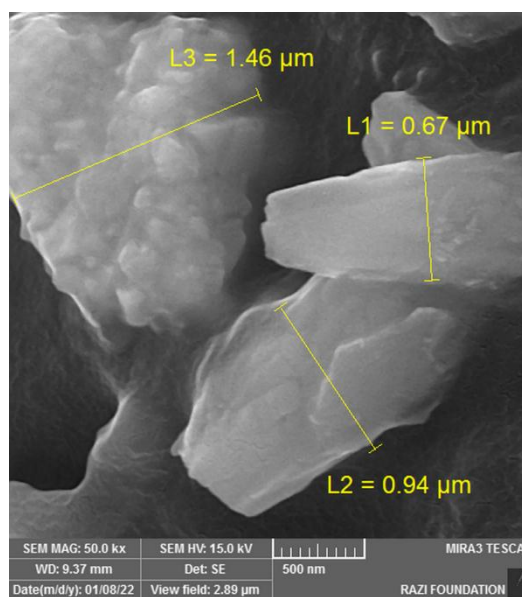
images clearly show the uniform distribution, good dispersion, and particle size of ZnO NPs. As illustrated in figure 9. (b), the particles exhibit a rod-like morphology with significantly larger dimensions within the matrix polymer [47].

Table 4. The mechanical properties of SBR/NR vulcanizates activated in the presence of ZnO NPs and industrial ZnO

Compound selection	M100 (MPa)	M300 (MPa)	T.S. (MPa)	E.B. (%)	Hardness (shore A)
SN0.5	0.745± 0.01	1.187± 0.01	11.71± 0.01	184± 10	83± 0.5
SN5I	0.741± 0.01	1.120± 0.01	10.12± 0.01	168± 10	81± 0.5



a) SBR/NR vulcanizates with ZnO NPs



b) SBR/NR vulcanizates with micro ZnO

Figure 9. FESEM images of ZnO NPs and micro ZnO in the SBR/NR vulcanizates.

Conclusion

This study utilized a green synthesis approach to produce ZnO nanoparticles (NPs) using an aqueous extract of *Aloysia citrodora* leaves. The addition of 0.5 phr ZnO NPs to SBR/NR resulted

in a shorter optimal curing time compared to the use of 5 phr conventional ZnO. This reduction in curing time is primarily attributed to the significantly larger specific surface area of ZnO NPs, which is six times greater than that of traditional ZnO. By reducing the amount of ZnO required in the formulations, the study also minimized certain adverse environmental impacts associated with ZnO usage. These outcomes stem from the unique properties of ZnO NPs, including their highly active surface, which outperforms commercial ZnO. The alkaline nature (pH = 12) of the green-synthesized ZnO NPs likely contributed to their improved curing behavior. Generally, biological methods for synthesizing ZnO nanoparticles are favored over physical and chemical methods due to their lower cost, energy consumption, and processing time. Additionally, the absence of chemical solvents and environmental pollutants is a significant advantage of this approach. The use of ZnO NPs as an activator in rubber compounds enhances the dispersion and compatibility of the nanoparticles within the polymer matrix, further improving the material's performance.

Acknowledgements

"This article has been conducted with the financial support of the Iran Small Industries and Industrial Parks Organization."

The authors are thankful to the Islamic Azad University, Yadegar-e-Imam, Shahre-Ray Branch and Shahr-e-Qods Branch for their support.

References:

1. Moradi, F., Sedaghat, S., Moradi, O. & Salmanabadi, S. A. Review on green nano-biosynthesis of silver nanoparticles and their biological activities: With an emphasis on medicinal plants. *Inorg. Nano-Metal Chem.* **51**, 133–142 (2021).
2. Hamrayev, H. & Shameli, K. Biopolymer-based green synthesis of zinc oxide (ZnO) nanoparticles. *IOP Conf. Ser.: Mater. Sci. Eng.* **012088** (2021).
3. Abel, S. et al. Green synthesis and characterizations of zinc oxide (ZnO) nanoparticles using aqueous leaf extracts of coffee (*Coffea arabica*) and its application in environmental toxicity reduction. *J. Nanomater.* **2021**, 1–6 (2021).
4. Mohamed Isa, E. D. et al. Variation of green synthesis techniques in fabrication of zinc oxide nanoparticles – A mini review. *IOP Conf. Ser.: Mater. Sci. Eng.* **1051**, 012001 (2021).
5. Vijayaraghavan, K. & Ashokkumar, T. Plant-mediated biosynthesis of metallic nanoparticles: A review of literature, factors affecting synthesis, characterization techniques and applications. *J. Environ. Chem. Eng.* **5**, 4866–4883 (2017).

6. Mohd Yusof, H. et al. Microbial synthesis of zinc oxide nanoparticles and their potential application as an antimicrobial agent and a feed supplement in animal industry: a review. *J. Anim. Sci. Biotechnol.* **10**, 57 (2019).
7. Vishnukumar, P., Vivekanandhan, S., Misra, M. & Mohanty, A. K. Recent advances and emerging opportunities in phytochemical synthesis of ZnO nanostructures. *Mater. Sci. Semicond. Process.* **80**, 143–161 (2018).
8. Zhang, L., Hua, J. & Wang, Z. Dynamically vulcanized polylactide/nitrile butadiene rubber blends with continuous cross-linked rubber phase. *J. Polym. Res.* **26**, 1–10 (2018).
9. Saputra, R. et al. Current progress in waste tire rubber devulcanization. *Chemosphere* **265**, 129033 (2021).
10. Nava, O. J. et al. Influence of *Camellia sinensis* extract on zinc oxide nanoparticle green synthesis. *J. Mol. Struct.* **1134**, 121–125 (2017).
11. Yu, H.-w. et al. Template-free hydrothermal synthesis of flower-like hierarchical zinc oxide nanostructures. *Optik* **168**, 778–783 (2018).
12. Fu, L. & Fu, Z. *Plectranthus amboinicus* leaf extract–assisted biosynthesis of ZnO nanoparticles and their photocatalytic activity. *Ceram. Int.* **41**, 2492–2496 (2015).
13. Salavati-Niasari, M., Davar, F. & Farhadi, M. Synthesis and characterization of spinel-type CuAl₂O₄ nanocrystalline by modified sol–gel method. *J. Sol-Gel Sci. Technol.* **51**, 48–52 (2009).
14. Aisida, S. O. et al. Bio-inspired encapsulation and functionalization of iron oxide nanoparticles for biomedical applications. *Eur. Polym. J.* **122**, 109371 (2020).
15. Vijayakumar, S. et al. Green synthesis of zinc oxide nanoparticles using *Atalantia monophylla* leaf extracts: Characterization and antimicrobial analysis. *Mater. Sci. Semicond. Process.* **82**, 39–45 (2018).
16. Rahaiee, S. et al. Green synthesis, characterization, and biological activities of saffron leaf extract-mediated zinc oxide nanoparticles: A sustainable approach to reuse an agricultural waste. *Appl. Organomet. Chem.* **34**, e5680 (2020).
17. Matinise, N. et al. ZnO nanoparticles via *Moringa oleifera* green synthesis: Physical properties & mechanism of formation. *Appl. Surf. Sci.* **406**, 339–347 (2017).
18. Sharmila, G. et al. Biosynthesis, characterization, and antibacterial activity of zinc oxide nanoparticles derived from *Bauhinia tomentosa* leaf extract. *J. Nanostruct. Chem.* **8**, 293–299 (2018).
19. Anjali, K. P. et al. Seaweed mediated fabrication of zinc oxide nanoparticles and their antibacterial, antifungal and anticancer applications. *ChemistrySelect* **6**, 647–656 (2021).
20. Hashemi, S., Asrar, Z., Pourseyedi, S. & Nadernejad, N. Green synthesis of ZnO nanoparticles by olive (*Olea europaea*). *IET Nanobiotechnol.* **10**, 400–404 (2016).
21. Çolak, H. & Karaköse, E. Green synthesis and characterization of nanostructured ZnO thin films using *Citrus aurantifolia* (lemon) peel extract by spin-coating method. *J. Alloys Compd.* **690**, 658–662 (2017).
22. Anbuvaran, M. et al. *Anisochilus carnosus* leaf extract mediated synthesis of zinc oxide nanoparticles for antibacterial and photocatalytic activities. *Mater. Sci. Semicond. Process.* **39**, 621–628 (2015).
23. Alyamani, A. A. et al. Green fabrication of zinc oxide nanoparticles using *Phlomis* leaf extract: Characterization and in vitro evaluation of cytotoxicity and antibacterial properties. *Molecules* **26**, 6142 (2021).

24. Susanna, A. et al. ZnO nanoparticles anchored to silica filler. A curing accelerator for isoprene rubber composites. *Chem. Eng. J.* **275**, 245–252 (2015).
25. Roy, K. et al. Sol–gel derived nano zinc oxide for the reduction of zinc oxide level in natural rubber compounds. *J. Sol-Gel Sci. Technol.* **70**, 378–384 (2014).
26. Mendoza, A. I. et al. Super-hydrophobic zinc oxide/silicone rubber nanocomposite surfaces. *Surf. Interfaces* **14**, 146–157 (2019).
27. He, Q. et al. Effects of two nano-ZnO processing technologies on the properties of rubber. *Appl. Nanosci.* **8**, 2009–2020 (2018).
28. Wang, Z. et al. Preparation of nano-zinc oxide/EPDM composites with both good thermal conductivity and mechanical properties. *J. Appl. Polym. Sci.* **119**, 1144–1155 (2011).
29. Mostoni, M. et al. Zinc-based curing activators: New trends for reducing zinc content in rubber vulcanization process. *Catalysts* **9**, 664 (2019).
30. Sienkiewicz, M. et al. Environmentally friendly polymer-rubber composites obtained from waste tyres: A review. *J. Clean. Prod.* **147**, 560–571 (2017).
31. Mostoni, S. et al. Design of a Zn single-site curing activator for a more sustainable sulfur cross-link formation in rubber. *Ind. Eng. Chem. Res.* **60**, 10180–10192 (2021).
32. Das, A. et al. Preparation of zinc oxide free, transparent rubber nanocomposites using a layered double hydroxide filler. *J. Mater. Chem.* **21**, 7194–7201 (2011).
33. Aisida, S. O. et al. Calcination effect on the photoluminescence, optical, structural, and magnetic properties of polyvinyl alcohol doped ZnFe₂O₄ nanoparticles. *J. Macromol. Sci. B* **59**, 295–308 (2020).
34. Madubuonu, N. et al. Bio-inspired iron oxide nanoparticles using *Psidium guajava* aqueous extract for antibacterial activity. *Appl. Phys. A* **126**, 1–10 (2020).
35. Ban, S. P. & Kumar, D. Synthesis, characterization and the application of ZnO nanoparticles in biotechnology. *Int. J. Adv. Chem. Eng. Biol. Sci.* **1**, 1–5 (2014).
36. Santhoshkumar, J. et al. Synthesis of zinc oxide nanoparticles using plant leaf extract against urinary tract infection pathogen. *Resour.-Effic. Technol.* **3**, 459–465 (2017).
37. Umavathi, S. et al. Green synthesis of ZnO nanoparticles for antimicrobial and vegetative growth applications: A novel approach for advancing efficient high quality health care to human wellbeing. *Saudi J. Biol. Sci.* **28**, 1808–1815 (2021).
38. Madhumitha, G. et al. Green synthesis, characterization and antifungal and photocatalytic activity of *Pithecellobium dulce* peel-mediated ZnO nanoparticles. *J. Phys. Chem. Solids* **127**, 43–51 (2019).
39. Degefa, A. et al. Green synthesis, characterization of zinc oxide nanoparticles, and examination of properties for dye-sensitive solar cells using various vegetable extracts. *J. Nanomater.* **2021**, 1–9 (2021).
40. Barzinjy, A. A. & Azeez, H. H. Green synthesis and characterization of zinc oxide nanoparticles using *Eucalyptus globulus* Labill. leaf extract and zinc nitrate hexahydrate salt. *SN Appl. Sci.* **2**, 1–10 (2020).
41. Panampilly, B. & Thomas, S. Nano ZnO as cure activator and reinforcing filler in natural rubber. *Polym. Eng. Sci.* **53**, 1337–1346 (2013).
42. Surya, I., Sukeksi, L. & Hayeemasae, N. Studies on cure index, swelling behaviour, tensile and thermooxidative properties of natural rubber compounds in the presence of alkanolamide. *IOP Conf. Ser.: Mater. Sci. Eng.* **309**, 012001 (2018).
43. Qin, X. et al. Enhancing the performance of rubber with nano ZnO as activators. *ACS Appl. Mater. Interfaces* **12**, 48007–48015 (2020).

44. Elango, N. et al. The effect of high loaded multiwall carbon nanotubes in natural rubber and their nonlinear material constants. *J. Nanomater.* **2017**, 1–15 (2017).
45. Maiti, M. et al. Influence of synthesized nano-ZnO on cure and physico-mechanical properties of SBR/BR blends. *Int. J. Ind. Chem.* **8**, 273–283 (2016).
46. Suntako, R. Effect of zinc oxide nanoparticles synthesized by a precipitation method on mechanical and morphological properties of the CR foam. *Bull. Mater. Sci.* **38**, 1033–1038 (2015).
47. Lin, Y. et al. Effect of ZnO nanoparticles doped graphene on static and dynamic mechanical properties of natural rubber composites. *Compos. Part A Appl. Sci. Manuf.* **70**, 35–44 (2015).

HOW TO CITE THIS ARTICLE

Monireh Alvand Ghiasvand, Sajjad Sedaghat, Mohammad Reza Allah Gholi Ghasri, Fereshteh Motiei, Farrokh Roya Nikmaram, “**Green nano bio-synthesis of ZnO/ styrene-butadiene rubber / natural rubber (SBR/ NR) nanocomposite and their assessment by use of curing time and mechanical properties**” International Journal of New Chemistry., 2025; 12(4), 754-773.